


RESEARCH ARTICLE

Relative contributions of local heat storage and ocean heat transport to cold-season Arctic Ocean surface energy fluxes in CMIP6 models

Khaled al Hajjar | Marc Salzmann Institute for Meteorology, Leipzig
University, Leipzig, Germany**Correspondence**Marc Salzmann, Institute for Meteorology,
Universität Leipzig, Leipzig, Germany.
Email: marc.salzmann@uni-leipzig.de**Funding information**Deutsche Forschungsgemeinschaft,
Grant/Award Number: 268020496**Abstract**

The Arctic near-surface air temperature increases most strongly during the cold season, and ocean heat storage has often been cited as a crucial component in linking the ice-albedo radiative feedback, which is active in summer, and near-surface air temperature increase in winter, when the lapse rate feedback contributes to Arctic warming. Here, we first estimate how much local heat storage and ocean heat transport contribute to net surface energy fluxes on a seasonal scale in CMIP6 models. We then compare contributions in a base state under weak anthropogenic forcing to a near-present-day state in which significant Arctic amplification is simulated. Our analysis indicates that, in a few regions, ocean heat transport plays a larger role for cold-season net surface energy fluxes compared with local heat storage. Analyzing differences between past and near-present-day conditions suggests that the lapse rate feedback, which mainly acts during the cold season in warm water inflow regions, may be more strongly influenced than previously thought by increased ocean heat transport from lower latitudes.

KEYWORDS

Arctic amplification, CMIP6, heat storage and transport

1 | INTRODUCTION

In an early global climate model study, Manabe and Wetherald (1975) found that surface air temperature at high latitudes responds more strongly to greenhouse gas warming compared with the global mean surface temperature. Since then, Arctic amplification (Holland and Bitz, 2003; Serreze and Francis, 2006; Pithan and Mauritsen, 2014; Previdi *et al.*, 2021) has clearly emerged in

the surface air temperature record (England *et al.*, 2021; Chylek *et al.*, 2022). During recent decades, Arctic surface air temperature has increased several times faster than the global mean temperature (Chylek *et al.*, 2022), and Arctic amplification has by now been recognized as a robust feature in climate model simulations and observations (England *et al.*, 2021). Evidence of Arctic amplification on Quaternary time scales has also emerged (Miller *et al.*, 2010; Park *et al.*, 2019).

This is an open access article under the terms of the [Creative Commons Attribution](https://creativecommons.org/licenses/by/4.0/) License, which permits use, distribution and reproduction in any medium, provided the original work is properly cited.

© 2023 The Authors. *Quarterly Journal of the Royal Meteorological Society* published by John Wiley & Sons Ltd on behalf of the Royal Meteorological Society.

Arctic amplification has often been attributed either to local feedbacks or to a combination of heat transport and local feedbacks, often with an emphasis on local feedbacks. In particular, the absence of efficient mixing of air at the surface and the sea ice retreat are understood to contribute to Arctic amplification (e.g. Manabe and Wetherald, 1975; Pithan and Mauritsen, 2014; Boeke *et al.*, 2021).

Effects of ocean heat transport on Arctic sea ice (see e.g. review by Docquier and Koenigk, 2021) have been investigated among others by Tsubouchi *et al.* (2020), Docquier *et al.* (2021), and Decuyper *et al.* (2022), and several studies suggested that ocean heat transport shapes polar climate change (Goosse *et al.*, 2018). Several studies (Koenigk and Brodeau, 2013; van der Linden *et al.*, 2019; Beer *et al.*, 2020) have also highlighted the role of ocean heat transport for Arctic amplification. The overall effect of ocean heat transport on Arctic amplification was, however, found to be small by Pithan and Mauritsen (2014) in a study that focused on radiative feedbacks. Instead, Pithan and Mauritsen (2014) point to the ocean as an important heat reservoir. The role of the Arctic Ocean as an important heat reservoir has recently also been highlighted in other studies on Arctic amplification (Dai *et al.*, 2019; Boeke *et al.*, 2021; Chemke *et al.*, 2021; Chung *et al.*, 2021; Dai, 2021; Jenkins and Dai, 2021; Liang *et al.*, 2022). In particular, the observation that Arctic amplification is strongest during the cold season whereas the sea-ice albedo feedback is active during summer points to ocean heat storage as a potentially important contributor to Arctic amplification. Several studies suggested that ocean heat release in winter helps to explain why Arctic amplification and the lapse rate feedback are strongest in winter (Pithan and Mauritsen, 2014; Boeke *et al.*, 2021; Chung *et al.*, 2021; Jenkins and Dai, 2021). The Arctic lapse rate feedback strongly depends on surface temperature changes (Boeke *et al.*, 2021; Jenkins and Dai, 2021) and arguably acts even when only the surface air temperature changes while the tropospheric temperature above the air near the surface remains constant (Salzmänn, 2017).

Although it is widely understood that the surface albedo feedback (due to sea ice changes) and the lapse rate feedback (due to a lack of efficient vertical mixing in the atmosphere) are important for Arctic amplification, and there is evidence that the lapse rate feedback is affected by ocean heat release in winter (Boeke *et al.*, 2021; Chung *et al.*, 2021; Jenkins and Dai, 2021), when solar absorption at the surface ceases, and that ocean heat transport is correlated with sea ice fraction (Årthun *et al.*, 2012), other aspects are less well understood. In particular, it is still unclear how much ocean heat transport contributes to ocean heat release in winter compared with ocean heat storage. On a more fundamental level, it is still unclear, whether changes in ocean heat transport can be

represented in terms of a closed feedback loop or should be classified as important drivers of polar climate change that cannot be expressed within a feedback framework (Goosse *et al.*, 2018). If the main role of the ocean in climate change were an increase of local seasonal heat storage and release, a local feedback framework (e.g. Pithan and Mauritsen, 2014; Chung *et al.*, 2021) would seem appropriate as far as the lapse rate feedback is concerned.

Although ocean heat release in winter is thought to play an important role for Arctic amplification, and although numerous previous studies have investigated heat transport to the Arctic, the relative importance of heat storage and heat transport for the cold-season surface energy release in warm water inflow regions has not been widely addressed. Consequently, it is still unclear whether the cold-season lapse rate feedback is indeed mainly related to local ocean heat storage (Pithan and Mauritsen, 2014; Boeke *et al.*, 2021; Chung *et al.*, 2021; Jenkins and Dai, 2021) and how strongly ocean heat transport from lower latitudes modulates this important feedback, as suggested by the geographical pattern of the lapse rate feedback (figure 1g of Boeke *et al.*, 2021), which tends to be strongest in warm water inflow regions, which are most strongly affected by changes in ocean heat release (Metzner *et al.*, 2020). Here, we investigate the relative contributions of ocean heat storage and ocean heat transport to winter surface energy fluxes based on several coupled climate models that participated in the Coupled Model Intercomparison Project Phase 6 (CMIP6, Eyring *et al.*, 2016). The first goal is to understand whether local heat storage or ocean heat transport is the main contributor to net positive upward surface energy fluxes during Arctic winter in these models, or whether both contribute equally. The second goal is to understand how these relative contributions change in a climate warming scenario and thus to help clarify whether ocean heat transport can be considered an important driver of Arctic climate change or whether a local feedback framework is more appropriate.

For historical simulations, several coupled climate models that participated in CMIP6 simulate Arctic amplification that is consistent with observation and reanalysis datasets (Davy *et al.*, 2018; Ye and Messori, 2021; Chylek *et al.*, 2022), although the ensemble spread tends to be large even for individual ensemble runs from the same model, and single-model ensemble averages tend to differ between models (e.g. Ye and Messori, 2021). As expected in the presence of internal variability, depending on the analysis period, the multi-model ensemble mean either agrees with or deviates from the observations due to internal variability (Chylek *et al.*, 2022). For a hypothetical perfect model, this is expected because internal variability affects observations but is averaged out when averaging over a

TABLE 1 Overview of Coupled Model Intercomparison Project Phase 6 model names and data used in this study,

Model name	Model reference	Data references	No. of runs (historical, ssp245)
ACCESS-CM2	Bi <i>et al.</i> (2020)	Dix <i>et al.</i> (2019a, 2019b)	5, 5
ACCESS-ESM1-5	Ziehn <i>et al.</i> (2020)	Ziehn <i>et al.</i> (2019a, 2019b)	40, 40
CESM2	Danabasoglu <i>et al.</i> (2020)	Danabasoglu (2019a, 2019b)	11, 3
CESM2-WACCM	Danabasoglu <i>et al.</i> (2020)	Danabasoglu (2019c, 2019d)	3, 5
CNRM-CM6-1	Voltaire <i>et al.</i> (2019)	Voltaire (2018, 2019a)	29, 6
CNRM-ESM2-1	S�ferian <i>et al.</i> (2019)	Seferian (2018, 2019b)	10, 10
CanESM5	Swart <i>et al.</i> (2019e)	Swart <i>et al.</i> (2019a, 2019d)	65, 50
CanESM5-CanOE	Christian <i>et al.</i> (2022)	Swart <i>et al.</i> (2019b, 2019c)	3, 3
EC-Earth3	D�scher <i>et al.</i> (2022)	EC-Earth Consortium (2019a, 2019b)	21, 21
EC-Earth3-CC	D�scher <i>et al.</i> (2022)	EC-Earth Consortium (2019c, 2021)	7, 7
FGOALS-g3	Li <i>et al.</i> (2020)	Li (2019a, 2019b)	6, 4
FIO-ESM-2-0	Bao <i>et al.</i> (2020)	Song <i>et al.</i> (2019a, 2019b)	3, 3
GISS-E2-1-G	Kelley <i>et al.</i> (2020)	NASA/GISS (2018a, 2020)	45, 9
GISS-E2-1-H	Kelley <i>et al.</i> (2020)	NASA/GISS (2018b, 2019a)	25, 9
GISS-E2-2-G	Rind <i>et al.</i> (2020)	NASA/GISS (2019b, 2019c)	11, 5
IPSL-CM6A-LR	Boucher <i>et al.</i> (2020)	Boucher <i>et al.</i> (2018, 2019)	33, 11
KACE-1-0-G	Lee <i>et al.</i> (2019)	Byun <i>et al.</i> (2019a, 2019b)	3, 3
MIROC-ES2L	Hajima <i>et al.</i> (2020)	Hajima <i>et al.</i> (2019), Tachiiri <i>et al.</i> (2019)	31, 30
MIROC6	Tatebe <i>et al.</i> (2019)	Tatebe and Watanabe (2018), Shiogama <i>et al.</i> (2019)	50, 3
MPI-ESM1-2-LR	Mauritsen <i>et al.</i> (2019)	Wieners <i>et al.</i> (2019a, 2019b)	30, 30
NorESM2-LM	Seland <i>et al.</i> (2020)	Seland <i>et al.</i> (2019a, 2019b)	3, 3
UKESM1-0-LL ^a	Sellar <i>et al.</i> (2019)	Good <i>et al.</i> (2019), Tang <i>et al.</i> (2019)	16, 5
UKESM1-0-LL ^b	Sellar <i>et al.</i> (2019)	Byun (2020), Shim <i>et al.</i> (2020)	2, 0

^aMet Office Hadley Centre.^bNational Institute of Meteorological Sciences and Korea Meteorological Administration.

sufficient number of model runs. Regarding heat transport to the Arctic, Madonna and Sand  (2021) found that CMIP6 models yielded results that are closer to observations compared with models that took part in the Coupled Model Intercomparison Project Phase 5.

In this study, we first analyze monthly mean climate model output data to estimate the relative contributions of ocean heat storage and ocean heat transport to net surface energy fluxes on a seasonal scale. We then analyze changes of these contributions, comparing contributions in a base state under weak anthropogenic forcing to a state in which significant Arctic amplification is simulated.

2 | DATASETS AND METHODOLOGY

2.1 | CMIP6 data

We analyzed data from several global climate models that participated in CMIP6 (CMIP6, Eyring *et al.*, 2016). In the

CMIP6 historical simulations, emissions of anthropogenic greenhouse gases and anthropogenic aerosol precursors are prescribed based on estimates of past emissions for the years 1850 to 2014. Effects of volcanic aerosols and solar variability are also taken into account. In the ssp245 scenario, anthropogenic emissions for the years 2014 to 2100 are assumed to follow a medium pathway, which sets this scenario apart from other high- and low-emission scenarios. Eyring *et al.* (2016) provide an overview of the CMIP6 model experiment set-up. Table 1 provides an overview of the model runs that were used in this study. We selected the models for which output data for at least three realizations for the ssp245 scenario including the corresponding historical runs were available. When computing a multimodel mean, we first combined the realizations for each model and then averaged, so that each model result is weighted identically independent of the number of realizations. We did not, however, combine results from similar models prior to computing the multimodel mean. For one of the models (UKESM1-0-LL; see Table 1), results were provided by two different groups. These results were

combined on the grounds that both groups ran the same model.

2.2 | Data analysis

2.2.1 | Computation of monthly mean surface energy fluxes

The local net upward energy flux at the surface F_{net} was computed as

$$F_{\text{net}} = R + \text{LHF} + \text{SHF},$$

where $R = \text{LW}_{\text{emi}} - \text{SW}_{\text{abs}} - \text{LW}_{\text{abs}}$ is the net radiative upward flux at the surface, LHF is the upward latent heat flux, and SHF is the upward sensible heat flux. LW_{emi} is emitted terrestrial (long-wave) radiation, SW_{abs} is absorbed solar (short-wave) radiation, and LW_{abs} is absorbed terrestrial radiation at the surface. SW_{abs} represents the difference between incoming and outgoing (reflected) solar radiation at the surface.

2.2.2 | Multiyear averaged annual cycle

Because we are interested in the annual cycle of surface energy fluxes, we computed multiyear mean annual cycles of surface energy fluxes from monthly mean data starting with March instead of January and ending with February instead of December. This reduces the length of a given multiyear time series by 12 months. The idea behind this is to reduce potential effects from mismatches at the beginning and end of the time series. When starting the averaging in December, there are always two Northern Hemisphere winter months at the beginning of the time series that do not correspond to any spring or summer months included in the time series. On the other hand, only one winter month at the end of a conventional multiyear time series corresponds to one full summer and fall. A mismatch between the winter months at the beginning of a time series and the winter month at the end, which may potentially influence multiyear averages, can then arise because of internal variability and/or long-term trends. Our decision to start time series analysis with March and end with February does not completely avoid the potential problem of a mismatch. But it is expected to reduce the potential impacts of remaining mismatches.

2.2.3 | Decomposition of surface energy fluxes

The multiyear mean monthly mean net upward surface energy flux can be either positive or negative. A positive

upward flux indicates that, in the monthly mean, energy is transferred from the surface toward the atmosphere. A negative upward flux indicates that the surface receives energy from above.

Based on the sign of the monthly mean net upward surface energy flux computed from the CMIP6 model output, we artificially decompose the multiyear mean monthly mean net upward energy flux into contributions from months in which, on average, the surface emits energy toward the atmosphere (here, F_{pos}) and months in which, on average, the surface receives energy (here, F_{neg}):

$$F_{\text{net}} = F_{\text{pos}} + F_{\text{neg}}, \quad (1)$$

where F_{pos} (F_{neg}) is the monthly mean net upward energy flux at the surface during a month with a monthly mean positive (negative) net upward energy flux at the surface.

We first computed the time mean annual cycle for each model run as described in Section 2.2.2. Then, we averaged the annual cycles from the different realizations to obtain the ensemble mean annual cycle for each model. The ensemble mean annual cycle was then decomposed into positive and negative contributions. In order to account for the variation of the number of days in a month, we weighted the monthly mean surface energy fluxes by the number of days in the specific month divided by one-twelfth of the number of days in the specific year. Multimodel means were computed by averaging over the results from this analysis.

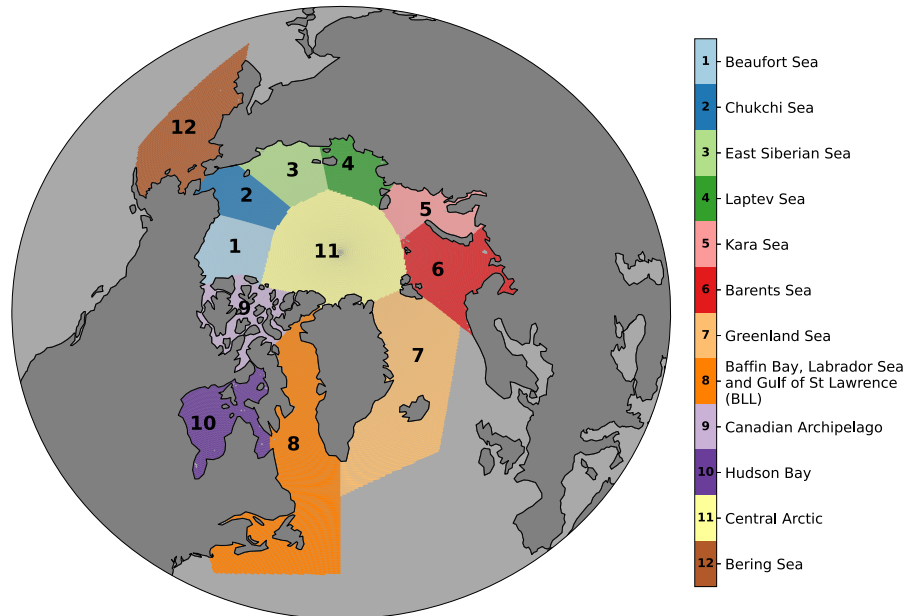
2.2.4 | Estimating contributions of local heat storage and other processes

In order to estimate the contribution of processes other than local heat storage to the seasonal surface energy flux from multiyear data containing complete 12-month cycles, we compute the ratio

$$r = \frac{|F_{\text{pos}}| - |F_{\text{neg}}|}{|F_{\text{pos}}| + |F_{\text{neg}}|} = \frac{F_{\text{net}}}{|F_{\text{pos}}| + |F_{\text{neg}}|}, \quad (2)$$

where $|F_x|$ denotes the absolute of F_x . The choice of the denominator in Equation (2) ensures that the ratios that will be shown in the maps (i.e., at grid scale) vary between -1 and $+1$. This denominator equals twice the seasonal ocean heat uptake plus ocean heat transport. For $r = 0$, the annual mean local net upward surface energy flux is zero and local heat storage dominates. For $r = -1$ or $r = 1$, one can assume that local heat storage plays only a minor role. The dominant process for $r = -1$, $r = 0$, and $r = 1$

FIGURE 1 Region masks based on Walsh *et al.* (2017) [Colour figure can be viewed at wileyonlinelibrary.com]



regarding the net surface energy flux are

$$r = \begin{cases} -1: & \text{surface receives energy} \\ 0: & \text{local heat storage} \\ 1: & \text{surface loses energy.} \end{cases}$$

One caveat of this interpretation is that r is computed from monthly mean data. It should therefore be regarded as a first-order estimate. On the one hand, since we are interested in the seasonal cycle, some filtering of high-frequency variability seems desirable. On the other hand, using high-frequency output data and an integral-preserving filter for smoothing would potentially lead to more exact results. However, in addition to limited data availability for daily data, this would still leave open the question of what exactly the filter time-scale should be, and it seems unlikely that the additional effort would result in fundamentally different results.

In order to determine in which direction r changes, we compute the difference:

$$d = r_2 - r_1, \quad (3)$$

where r_2 is r for March 2000 to February 2050 and r_1 is r for March 1850 to February 1900. For computing r_2 , we use ssp245 runs (starting with the year 2015) together with the corresponding historical runs (up to the year 2014). By corresponding run, we mean the run that provides the initial conditions; that is, the “parent” run. For computing r_1 , we take into account only the historical runs that served as a starting point for the ssp245 runs. For each ssp245 run, we combine the ssp245 run and the corresponding historical run into one time series. We then analyze time slices from these combined time series. For regions with positive r , a

positive d implies an increased contribution of ocean heat transport to winter surface upward energy fluxes relative to local heat storage.

2.2.5 | Definition of subregions

We define Arctic Ocean subregions based on a mask that was originally devised for the “Sea Ice Back To 1850” dataset (Walsh *et al.*, 2017). The regions are shown in Figure 1.

3 | RESULTS

3.1 | Arctic net upward surface energy fluxes in CMIP6 models

Figure 2 shows multiyear mean net upward surface energy fluxes from the CMIP6 models listed in Table 1 for historical model runs. Positive net upward surface energy fluxes indicate that, on average, the surface emits energy and acts to heat the atmosphere. In the absence of a significant heat source inside the Arctic Ocean, positive net upward surface energy fluxes over a multiyear period can only be sustained by ocean heat transport. Another potential candidate would be the freezing of liquid water, during which heat is released. Melting sea ice, on the other hand, requires energy. Negative upward (i.e., positive downward) surface energy fluxes indicate that, on average, energy is taken up by the ocean or sea ice at the surface.

Negative multiyear mean net upward surface energy fluxes in Figure 2 are found in the Gulf of St Lawrence,

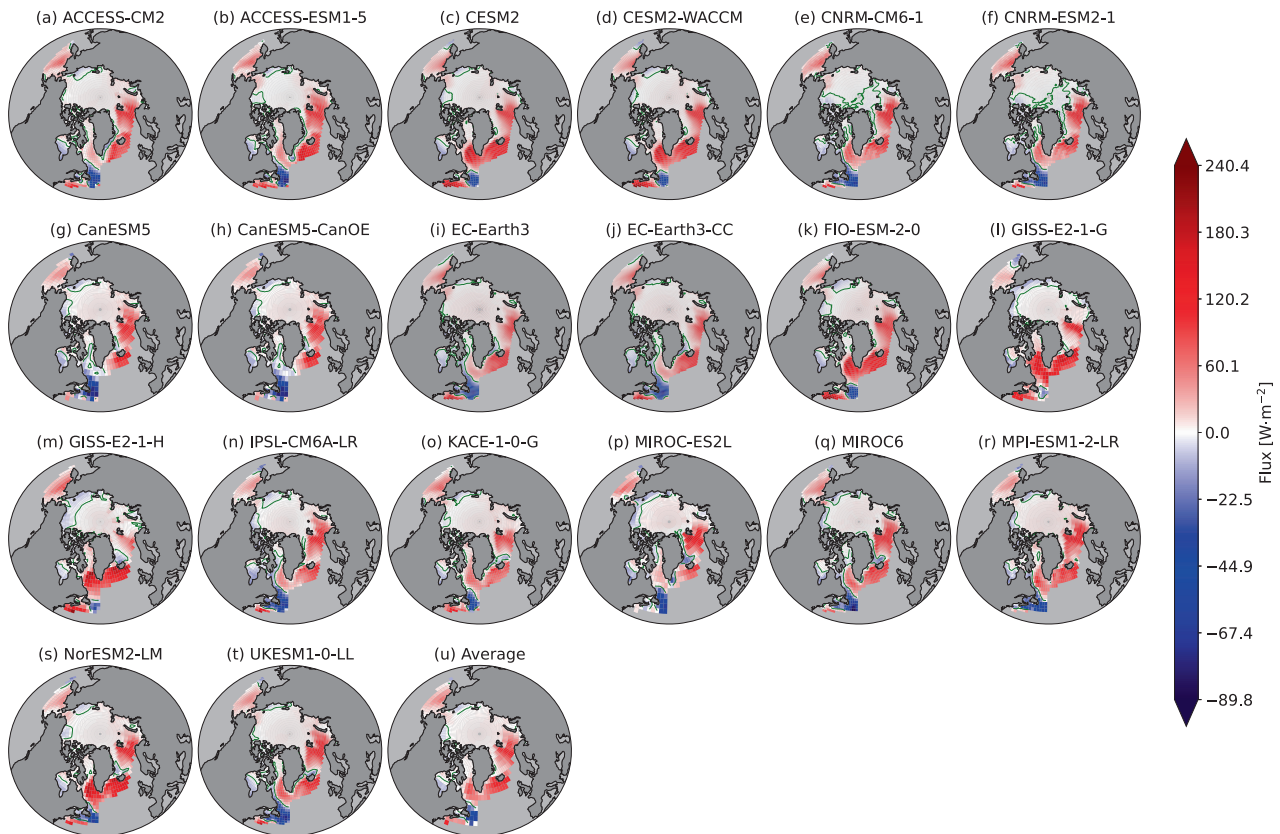


FIGURE 2 Ensemble mean time mean net upward surface energy flux for the period from March 1850 to February 2014 from various Coupled Model Intercomparison Project Phase 6 (CMIP6) models for all the regions defined in Figure 1. Based on CMIP6 historical simulations

the southern Labrador Sea, much of Hudson Bay, and in many of the models in parts of the Beaufort Sea and the East Siberian Sea as well. Long-term average net transfer of energy via the atmosphere to the Arctic Ocean is found mainly at higher latitudes outside the main warm water inflow in the marginal seas.

The net surface energy fluxes in the central Arctic, the Beaufort Sea, the Chukchi Sea, and the East Siberian Sea in Figure 2 are generally small. Especially for the central Arctic, this is expected due to sea ice cover persisting throughout the year in the historical runs. Most models compute slightly positive net upward surface energy fluxes over the central Arctic which may, for example, result from heat conduction through the sea ice, from leads, which are usually parametrized in global climate models, or, depending on the region, also from intermittent sea-ice-free conditions, in combination with ocean heat transport. Only the two Centre National de Recherches Météorologiques (CNRM) models (Figure 2e,f) show regions of slightly negative net upward surface energy fluxes extending into the central Arctic.

At depth, inflow of warm Atlantic water affects the entire Arctic Ocean (e.g. Carmack *et al.*, 2015). At the surface, the main signatures of warm Atlantic water are

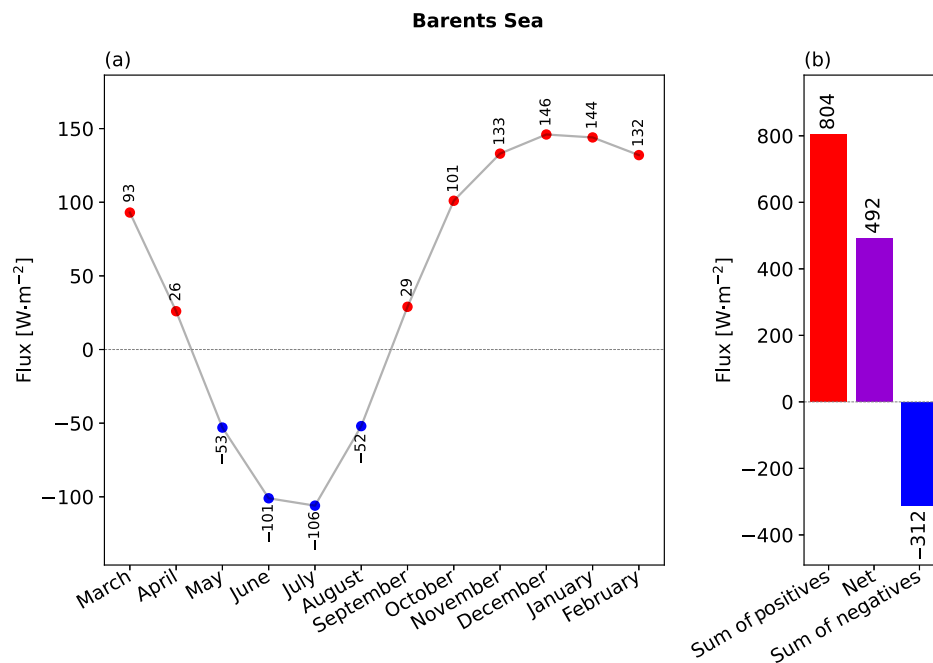
found in the Barents Sea, where warm water subsides and then further circulates across almost the entire Arctic Ocean. In most of the Greenland Sea and in southern parts of the Labrador Sea, where cold water from the Arctic Ocean flows southward and subsides below warmer Atlantic water, on average, the ocean acts to heat the atmosphere as well. This is evidenced by positive net upward surface energy fluxes in Figure 2. Warm water from the Pacific enters from the Bering Sea into the Chukchi Sea, resulting in average positive net upward surface energy fluxes in the Bering Sea and the Chukchi Sea.

3.2 | Contributions of ocean heat storage and ocean heat transport to surface energy fluxes on a seasonal scale in CMIP6 models by region

3.2.1 | Example: Barents Sea in the CanESM5 model

We now decompose the monthly mean data into data from months with positive and months with negative net upward surface energy fluxes. An example for the

FIGURE 3 (a) Mean over the period from March 1850 to February 2014 of the weighted monthly mean net upward surface energy flux from the CanESM5 model for the Barents Sea (ensemble mean). (b) Sum of monthly mean positive net upward surface energy fluxes, net upward surface energy flux, and sum of monthly mean negative net upward surface energy fluxes based on the the March to February mean annual cycle. [Colour figure can be viewed at wileyonlinelibrary.com]



Barents Sea from one of the CMIP6 models is shown in Figure 3. The multiyear average annual cycle for the period from March 1850 to February 2014 shows positive energy upward fluxes from the ocean toward the atmosphere from September to March. From May to August, the multiyear mean net upward surface energy fluxes are negative. The sum of the positive and negative net upward surface energy fluxes corresponds to the net upward energy flux over the period from March 1850 to February 2014 in Figure 3b. If we assume that the seasonal components must balance in the multiyear mean, in the absence of a heat source inside the ocean, this multiyear average net upward surface energy flux must be supplied by ocean heat transport.

Figure 3b therefore suggests that the contribution from ocean heat transport to the sum of the monthly mean positive fluxes is larger than the contribution from local ocean heat uptake during summer. In this particular example for the Barents Sea, ocean heat storage appears to account for less than half of the positive net upward surface energy flux from September to March.

3.2.2 | Multimodel spread

Before analyzing multimodel means in the next section, we investigate the spread between different models in this section. In Figure 4, we focus on the Barents Sea, the Beaufort Sea, the central Arctic, and the Chukchi Sea. Similar plots for the remaining regions are shown in Supporting Information Figures S1 and S2.

In the Barents Sea (Figure 4a), ocean heat transport contributes more to the sum of the positive net upward

surface energy fluxes than seasonal ocean heat storage in all the model simulations except the Goddard Institute for Space Studies (GISS) model family and KACE-1-0-G. On the whole, the results for net upward surface energy fluxes in the Barents Sea are qualitatively similar in the various model simulations, except that the net fluxes in the GISS model family and to some extent also KACE-1-0-G are smaller. The large multiyear net upward surface energy fluxes in the majority of the models confirm the importance of warm water inflow in the Barents Sea in the model simulations.

The Beaufort Sea is characterized by very small net surface energy fluxes and a moderate annual cycle of net surface energy fluxes in all the models (Figure 4b). Throughout most of the historical simulations, the Beaufort Gyre is characterized by particularly thick sea ice, which limits surface energy fluxes. Monthly mean positive and negative net upward surface energy fluxes almost balance each other in all the models. On the whole, the results are qualitatively similar across the models.

In the central Arctic (Figure 4c), the amplitude of the seasonal cycle of the net upward surface energy fluxes is again much smaller than in the Barents Sea (Figure 4a). Net surface energy fluxes per unit area are also smaller in magnitude than in the Barents Sea, which is in line with a larger annual mean sea-ice cover. Ocean heat transport from lower latitudes tends to play a lesser role in the central Arctic relative to local heat storage. Yet, in most models, ocean heat transport plays a non-negligible role for the decomposed positive net upward surface energy fluxes even in the central Arctic. An exception are the two CNRM models that showed negative net upward surface

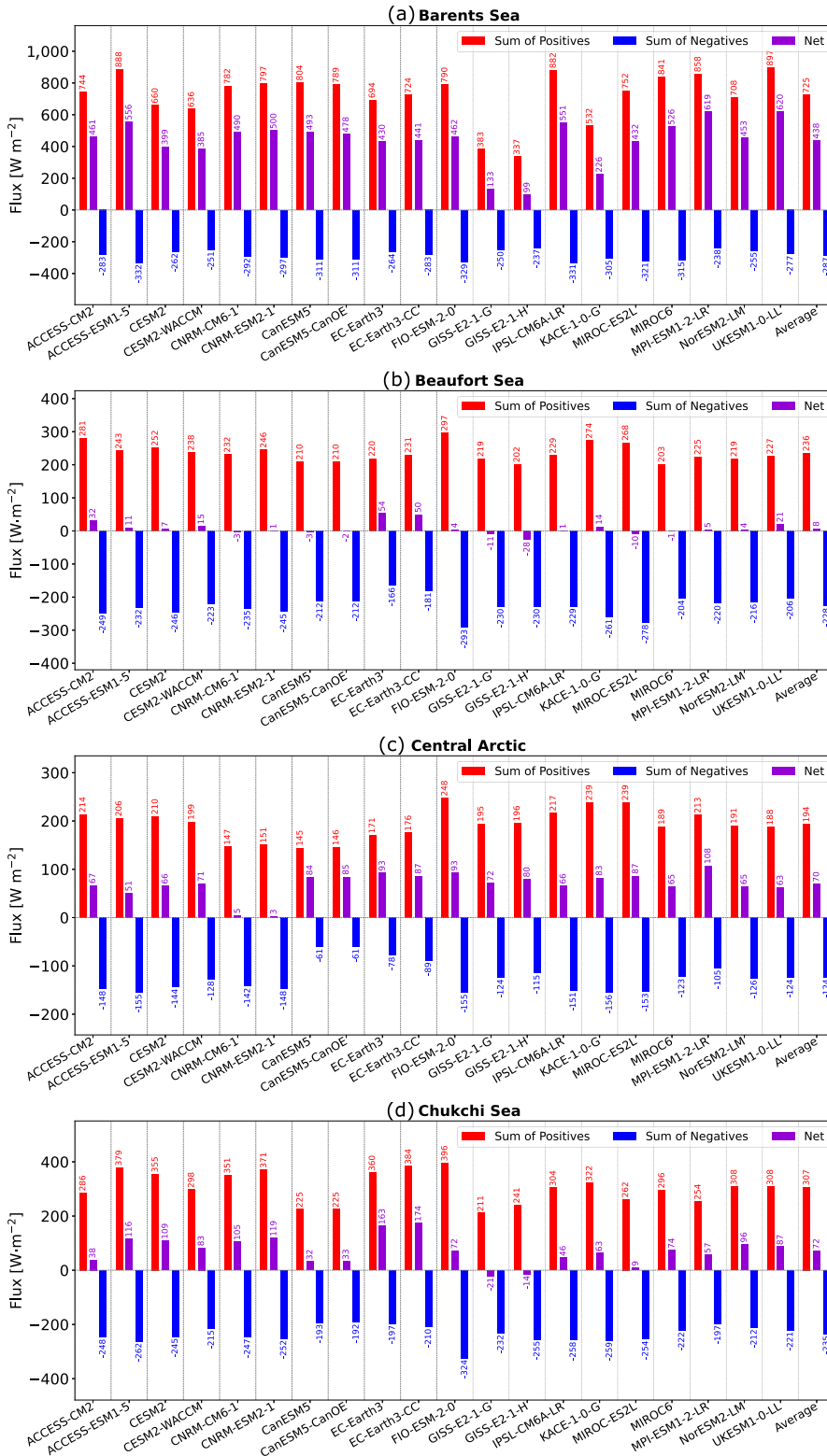


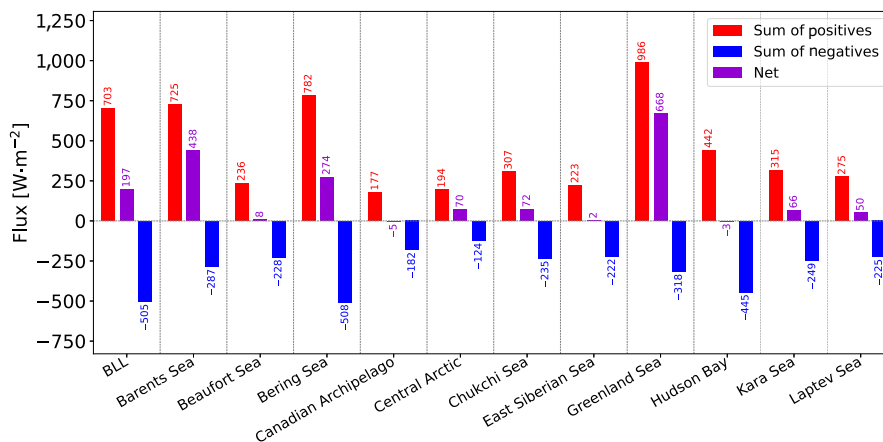
FIGURE 4 Sum of monthly mean positive net upward surface energy fluxes, net upward surface energy flux, and sum of monthly mean negative net upward surface energy fluxes as in Figure 3b from various Coupled Model Intercomparison Project Phase 6 models for (a) Barents Sea, (b) Beaufort Sea, (c) central Arctic, and (d) Chukchi Sea. [Colour figure can be viewed at wileyonlinelibrary.com]

energy fluxes in parts of the central Arctic in Figure 2. In these models, regional compensation results in small area-average net upward surface energy fluxes over the central Arctic.

Figure 4d for the Chukchi Sea shows again non-negligible long-term net surface energy fluxes, which are consistent with inflow of warmer water, in this case

especially from the Pacific through the Bering Strait. However, unlike in the Barents Sea, heat storage contributes more to the monthly mean positive net upward surface energy fluxes compared with ocean heat transport. Though the Arctic Ocean is comparatively well connected with the Atlantic, the Bering Strait is relatively shallow and relatively narrow.

FIGURE 5 Multimodel means: sum of monthly mean positive net upward surface energy fluxes, net upward surface energy flux, and sum of monthly mean negative net upward surface energy fluxes for the regions in Figure 1. BLL: Baffin Bay, Labrador Sea, and Gulf of St Lawrence. [Colour figure can be viewed at wileyonlinelibrary.com]



3.2.3 | Multimodel regional mean analysis

Figure 5 shows multi-model mean values of net upward surface energy fluxes for various regions, again including a decomposition into contributions from months with positive and months with negative net upward surface energy flux. Focusing on the four regions with the largest sums of monthly mean positive upward surface energy fluxes in Figure 5, one finds large contributions from ocean heat transport in each of them. The Barents Sea and the Greenland Sea stand out in that these are the only two regions in which the net upward surface energy flux is larger than the absolute of the sum of the monthly mean negative upward surface energy fluxes. This speaks to the importance of ocean heat transport for supporting the large positive upward surface energy fluxes in these regions. As one moves along the main import pathways of warm water from the Atlantic and the Pacific, ocean heat transport becomes less important relative to seasonal heat storage.

Our simple method to estimate the contribution of ocean heat transport to seasonal net upward surface energy fluxes yields values above 20% in the majority of the marginal seas. The Beaufort Sea and the East Siberian Sea are exceptions. Especially the Beaufort Sea away from the coast is characterized by robust sea-ice coverage. The Beaufort Sea and the East Siberian Sea are both outside the main inflow of warm Atlantic water. No notable net enhancement of simulated annual mean surface energy fluxes due to the influence of ocean heat transport is found in the Canadian Archipelago and Hudson Bay.

3.3 | Ratio of non-local to local contributions

In order to provide some rough visual guidance to the qualitative importance of non-local versus local contributions to seasonal net surface energy fluxes, we computed

the ratio r of net upward surface energy flux to the sum over the monthly mean positive and the absolute of the monthly mean negative net upward surface energy fluxes as defined in Equation (2). The pattern of r in Figure 6 is largely in line with the discussion of the results from the preceding analysis of regional net upward surface energy fluxes.

Warm water inflow regions show fairly large positive r , indicating a prominent contribution of ocean heat transport to the monthly mean net upward surface energy fluxes that occur in the colder part of the year. Negative r implies that net energy flux via the atmosphere to the ocean and sea ice plays a role. Small r means that local heat storage is large compared with the net upward surface energy flux. The main finding in Figure 6 is the large regions in which r is not overly small.

For much of the Arctic, r is positive, because the net surface energy flux in the numerator is positive, indicating that in the multiyear mean the energy is transferred from the ocean and sea ice toward the atmosphere. In warm water inflow regions, the contribution of ocean heat transport to monthly mean positive net upward surface energy fluxes can be of similar magnitude to the seasonal heat storage, as indicated by the preceding regional analysis and reflected in the darker red colors in Figure 6. In these regions, r would be even larger if only positive net upward surface energy fluxes were included in the denominator in Equation (2). Instead, the denominator contains the net flux and twice the (balanced) contribution due to seasonal heat storage, as defined by the sums of the absolute values of the positive and the negative monthly mean net upward surface energy fluxes.

Figure 6 also shows limited regional compensation occurring within the Baffin Bay, Labrador Sea, and Gulf of St Lawrence (BLL) region. This indicates that the preceding analysis of regional net upward surface energy fluxes for this particular region would have benefited from a region mask in which the BLL region is further subdivided into individual regions.

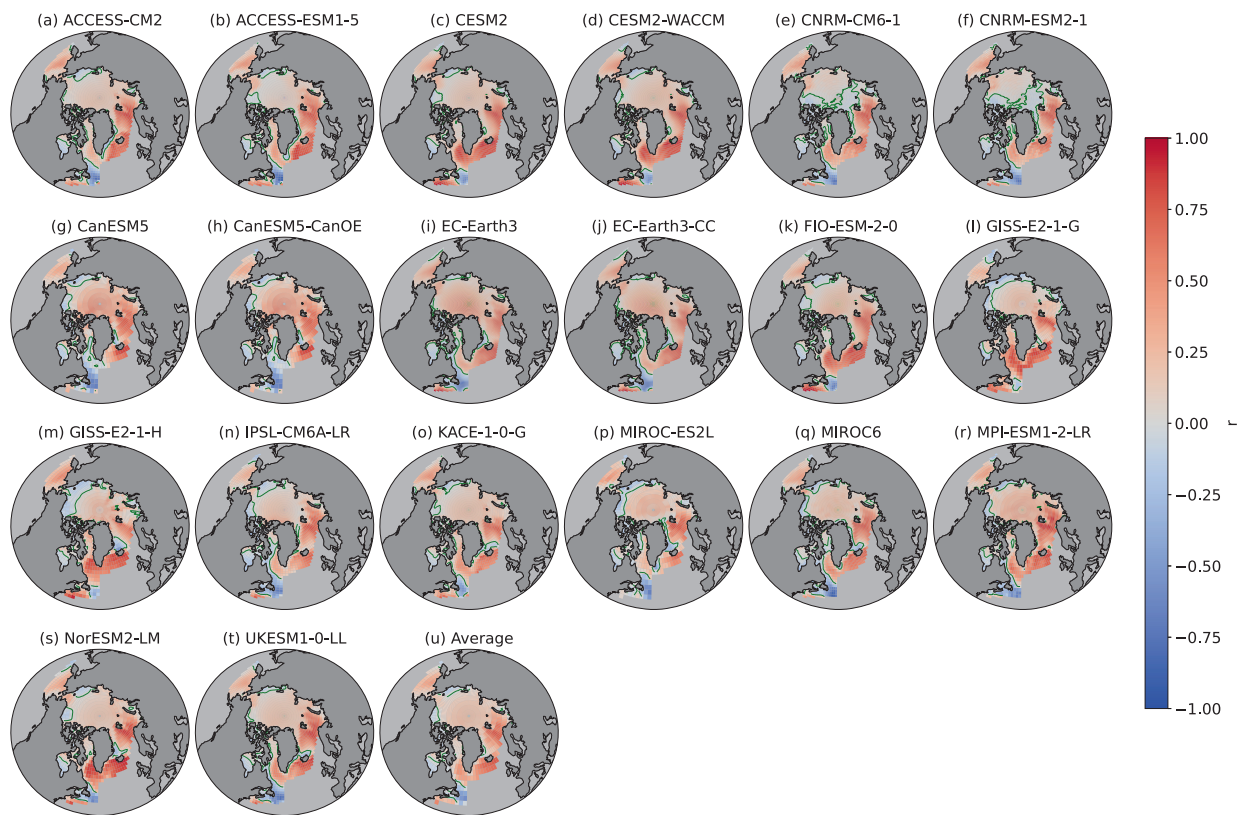


FIGURE 6 Ratio r of net upward surface energy flux to the sum over the monthly mean positive and the absolute of the monthly mean negative net upward surface energy fluxes as defined in Equation (2)

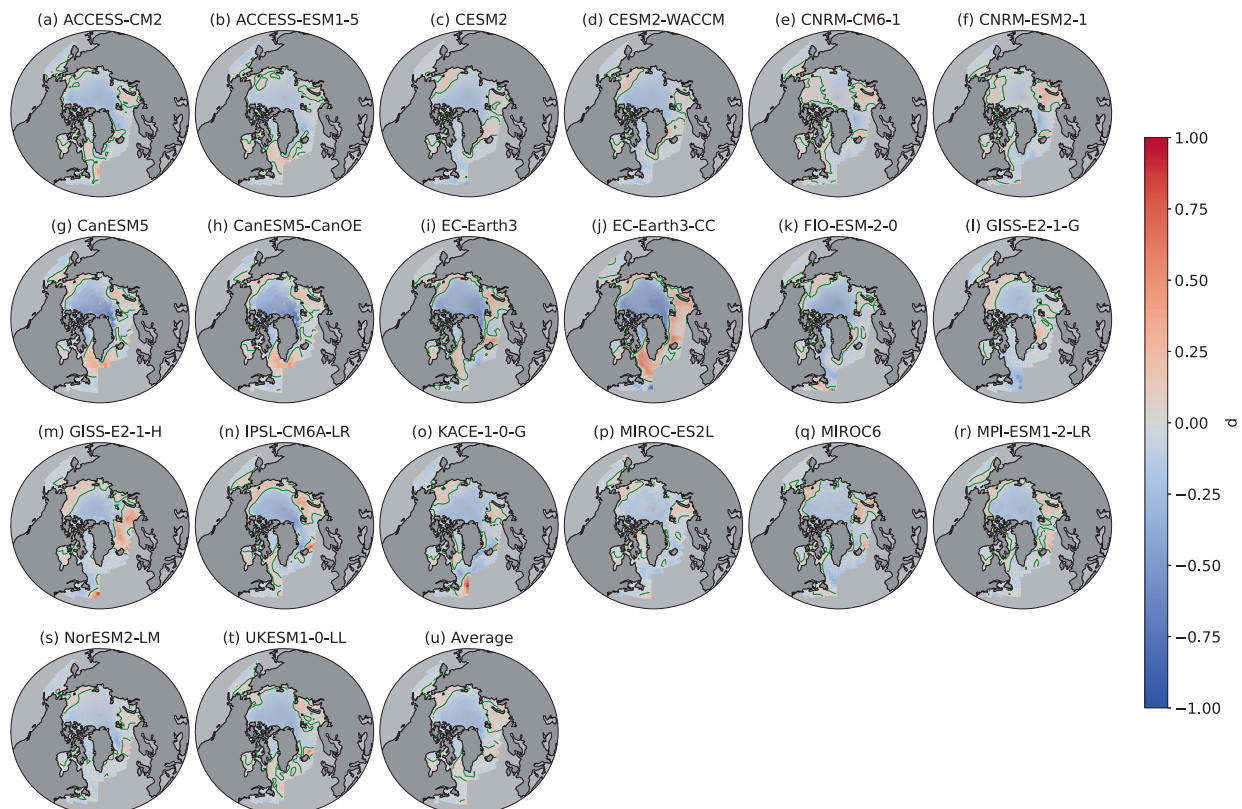


FIGURE 7 Difference d between r for March 2000 to February 2050 and r for March 1850 to February 1900

The main disadvantage of r is that a large part of the information in the previous sections is lost when focusing exclusively on this ratio.

3.4 | Comparison between the past and near-present-day

Comparing differences of the ratio r between the past and near-present-day conditions allows us to qualitatively analyze whether seasonal heat storage has become more or less important relative to non-local processes in a warmer climate with significant Arctic amplification. Figure 7 shows the difference d between r for March 2000 to February 2050 and r for March 1850 to February 1900, before Arctic amplification started to emerge. Red colors are found in regions that are strongly influenced by ocean heat transport and in which annually averaged positive net upward surface energy fluxes are typical (cf. Figure 2). This indicates that in a near-present-day climate, annual mean net upward surface energy fluxes, which are driven by ocean heat transport, take a more prominent role relative to seasonal heat storage in these regions. Blue colors indicate that the net upward surface energy fluxes have decreased and/or the seasonal heat storage contributes more strongly to the denominator. In either case, the contribution of ocean heat transport to the net surface fluxes has decreased compared with either seasonal heat storage and/or energy transfer via the atmosphere to the ocean.

Blue colors in the central Arctic Figure 7 are largely compatible with increased downward surface energy fluxes during summer and increased seasonal ocean heat storage. However, Figure 7 suggests that, for many of the models, ocean heat transport plays an increasingly important role in parts of the marginal seas.

4 | CONCLUSION

We analyzed the relative contributions of seasonal heat storage and ocean heat transport to net upward surface energy fluxes in the Arctic Ocean in CMIP6 models. Our analysis was based on a simple decomposition of net upward surface energy fluxes into contributions from months with positive and months with negative net upward surface energy fluxes and on the argument that, in the absence of significant local heat sources in the Arctic Ocean, long-term annual mean net upward energy fluxes can only be explained by ocean heat transport.

Our analysis suggests that, in the CMIP6 models, on average, ocean heat transport contributes more strongly to seasonal positive net upward surface energy fluxes than seasonal heat storage in the Greenland Sea and the Barents

Sea. Ocean heat transport was found to play an important role in other regions that are directly influenced by warm water inflow from higher latitudes as well, most notably the Bering Sea and the BLL region. Based on our simple method, we estimate the contribution of ocean heat transport to seasonal net upward surface energy fluxes to be above 20% in the majority of the marginal seas. A non-negligible contribution of ocean heat transport to seasonal net upward surface energy fluxes was also found in the central Arctic. In the East Siberian Sea, the Canadian Archipelago, Hudson Bay, and the Beaufort Sea the contribution of ocean heat transport to seasonal net upward surface energy fluxes was found to be very small in the multimodel average.

We also analyzed changes of the contributions of seasonal heat storage and ocean heat transport to net upward surface energy fluxes in the Arctic Ocean in CMIP6 models in a near-present-day climate compared with a reference period in which Arctic amplification had not yet emerged. We found a decreasing contribution of ocean heat transport to the net upward surface energy fluxes in the central Arctic, which is in line with increased downward surface energy fluxes during summer and increased seasonal ocean heat storage. However, in parts of the marginal seas, ocean heat transport plays an increasingly important role relative to seasonal ocean heat storage for positive net upward surface energy fluxes during the colder seasons.

As noted in Section 1, several previous studies have pointed out that ocean heat release in winter plays an important role for Arctic amplification and specifically also for the lapse rate feedback. A number of studies have, however, attributed this increased ocean heat release in winter mainly to increased ocean heat storage, whereas other studies have also highlighted the role of ocean heat transport. Our goal, therefore, was to compare the contributions of ocean heat storage and ocean heat transport to surface energy fluxes in winter in CMIP6 models, in part because such models are frequently being used in studies of Arctic amplification.

Our analysis indicates that not only increased ocean heat storage constitutes a quantitatively relevant contribution to increased surface warming in winter. In some warm water inflow regions, ocean heat transport is more important for winter surface energy fluxes than ocean heat storage, and for some regions winter ocean heat transport increases even more than ocean heat storage. Based on this outcome, together with the previous findings that ocean heat release in winter plays an important role for Arctic amplification (Dai *et al.*, 2019; Boeke *et al.*, 2021; Chemke *et al.*, 2021; Chung *et al.*, 2021; Dai, 2021; Jenkins and Dai, 2021; Liang *et al.*, 2022), affects the lapse rate feedback (Pithan and Mauritsen, 2014; Boeke *et al.*, 2021; Jenkins and Dai, 2021), and that the lapse rate feedback

is especially strong in warm water inflow regions during the cold season (Boeke *et al.*, 2021), we conclude that both increased heat storage and ocean heat transport contribute to the lapse rate feedback and Arctic amplification. This finding is of direct relevance to answering the question as to whether changes in ocean heat transport can be represented in terms of a closed feedback loop or should be classified as important drivers of polar climate change that cannot be expressed within a feedback framework (Goosse *et al.*, 2018). However, because atmospheric heat transport tends to increase whenever ocean heat transport decreases, one can still find Arctic amplification in the absence of ocean heat transport; for example, in coupled models in which an atmosphere model is coupled to a slab-ocean model (Chemke *et al.*, 2021). Polar amplification in models occurs even when placing a continent with a flat surface in the southern high latitudes, preventing not only ocean heat transport but also ocean heat storage (Salzmänn, 2017; Hahn *et al.*, 2020; Singh and Polvani, 2020).

ACKNOWLEDGEMENTS

We acknowledge the World Climate Research Programme, which, through its Working Group on Coupled Modelling, coordinated and promoted CMIP6. We thank the climate modeling groups for producing and making available their model output, the Earth System Grid Federation (ESGF) for archiving the data and providing access, and the multiple funding agencies who support CMIP6 and ESGF. CMIP6 data are available at <https://esgf-node.llnl.gov/projects/cmip6/>. The subregion mask from the SIBT1850 dataset is available at <https://nsidc.org/data/g10010>.

We gratefully acknowledge the funding by the Deutsche Forschungsgemeinschaft (German Research Foundation) – Project-ID 268020496 – TRR 172 within the Transregional Collaborative Research Center Arctic Amplification: Climate Relevant Atmospheric and Surface Processes, and Feedback Mechanisms (AC)³. Open Access funding enabled and organized by Projekt DEAL.

ORCID

Marc Salzmann  <https://orcid.org/0000-0002-3987-2303>

REFERENCES

- Årthun, M., Eldevik, T., Smedsrud, L.H., Skagseth, Ø. and Ingvaldsen, R.B. (2012) Quantifying the influence of Atlantic heat on Barents Sea ice variability and retreat. *Journal of Climate*, 25(13), 4736–4743.
- Bao, Y., Song, Z. and Qiao, F. (2020) FIO-ESM version 2.0: model description and evaluation. *Journal of Geophysical Research: Oceans*, 125(6). <https://doi.org/10.1029/2019jc016036>
- Beer, E., Eisenman, I. and Wagner, T.J.W. (2020) Polar amplification due to enhanced heat flux across the halocline. *Geophysical Research Letters*, 47, 4.
- Bi, D., Dix, M., Marsland, S., O'Farrell, S., Sullivan, A., Bodman, R., Law, R., Harman, I., Srbiniy, J., Rashid, H.A., Dobrotoff, P., Mackallah, C., Yan, H., Hirst, A., Savita, A., Dias, F.B., Woodhouse, M., Fiedler, R. and Heerdegen, A. (2020) Configuration and spin-up of ACCESS-CM2, the new generation Australian Community Climate and Earth System Simulator coupled model. *Journal of Southern Hemisphere Earth Systems Science*, 70(1), 225.
- Boeke, R.C., Taylor, P.C. and Sejas, S.A. (2021) On the nature of the Arctic's positive lapse-rate feedback. *Geophysical Research Letters*, 48(1). <https://doi.org/10.1029/2020GL091109>
- Boucher, O., Denvil, S., Levvasseur, G., Cozic, A., Caubel, A., Foujols, M.-A., Meurdesoif, Y., Cadule, P., Devilliers, M., Dupont, E. and Lurton, T. (2019) IPSL IPSL-CM6A-LR model output prepared for CMIP6 ScenarioMIP ssp245. *Versions*, 20190119, 20190516, 20191121, 20191003, 20200218.
- Boucher, O., Denvil, S., Levvasseur, G., Cozic, A., Caubel, A., Foujols, M.-A., Meurdesoif, Y., Cadule, P., Devilliers, M., Ghattas, J., Lebas, N., Lurton, T., Mellul, L., Musat, I., Mignot, J. and Cheruy, F. (2018) IPSL IPSL-CM6A-LR model output prepared for CMIP6 CMIP historical. *Versions*, 20180803, 20190802–20211229.
- Boucher, O., Servonnat, J., Albright, A.L., Aumont, O., Balkanski, Y., Bastrikov, V., Bekki, S., Bonnet, R., Bony, S., Bopp, L., Braconnot, P., Brockmann, P., Cadule, P., Caubel, A., Cheruy, F., Codron, F., Cozic, A., Cugnet, D., D'Andrea, F., Davini, P., Lavergne, C., Denvil, S., Deshayes, J., Devilliers, M., Ducharne, A., Dufresne, J.-L., Dupont, E., Éthé, C., Fairhead, L., Falletti, L., Flavoni, S., Foujols, M.-A., Gardoll, S., Gastineau, G., Ghattas, J., Grandpeix, J.-Y., Guenet, B., Lionel, E.G., Guilyardi, E., Guimberteau, M., Hauglustaine, D., Hourdin, F., Idelkadi, A., Joussaume, S., Kageyama, M., Khodri, M., Krinner, G., Lebas, N., Levvasseur, G., Lévy, C., Li, L., Lott, F., Lurton, T., Luyssaert, S., Madec, G., Madeleine, J.-B., Maignan, F., Marchand, M., Marti, O., Mellul, L., Meurdesoif, Y., Mignot, J., Musat, I., Ottlé, C., Peylin, P., Planton, Y., Polcher, J., Rio, C., Rochetin, N., Rousset, C., Sepulchre, P., Sima, A., Swingedouw, D., Thiéblemont, R., Traore, A.K., Vancoppenolle, M., Vial, J., Vialard, J., Viovy, N. and Vuichard, N. (2020) Presentation and evaluation of the IPSL-CM6a-LR climate model. *Journal of Advances in Modeling Earth Systems*, 12(7).
- Byun, Y.-H. (2020) NIMS-KMA UKESM1.0-LL model output prepared for CMIP6 CMIP historical. *Versions*, 20200205, 20200805.
- Byun, Y.-H., Lim, Y.-J., Shim, S., Sung, H.M., Sun, M., Kim, J., Kim, B.-H., Lee, J.-H. and Moon, H. (2019a) NIMS-KMA KACE1.0-G model output prepared for CMIP6 ScenarioMIP ssp245.
- Byun, Y.-H., Lim, Y.-J., Sung, H.M., Kim, J., Sun, M. and Kim, B.-H. (2019b) NIMS-KMA KACE1.0-G model output prepared for CMIP6 CMIP historical.
- Carmack, E., Polyakov, I., Padman, L., Fer, I., Hunke, E., Hutchings, J., Jackson, J., Kelley, D., Kwok, R., Layton, C., Melling, H., Perovich, D., Persson, O., Ruddick, B., Timmermans, M.-L., Toole, J., Ross, T., Vavrus, S. and Winsor, P. (2015) Toward quantifying the increasing role of oceanic heat in sea ice loss in the new Arctic. *Bulletin of the American Meteorological Society*, 96, 2079–2105.
- Chemke, R., Polvani, L.M., Kay, J.E. and Orbe, C. (2021) Quantifying the role of ocean coupling in Arctic amplification and sea-ice loss over the 21st century. *NPJ Climate and Atmospheric Science*, 4(1). <https://doi.org/10.1038/s41612-021-00204-8>

- Christian, J.R., Denman, K.L., Hayashida, H., Holdsworth, A.M., Lee, W.G., Riche, O.G.J., Shao, A.E., Steiner, N. and Swart, N.C. (2022) Ocean biogeochemistry in the Canadian Earth System Model version 5.0.3: CanESM5 and CanESM5-CanOE. *Geoscientific Model Development*, 15(11), 4393–4424.
- Chung, E.-S., Ha, K.-J., Timmermann, A., Stuecker, M.F., Bodai, T. and Lee, S.-K. (2021) Cold-season Arctic amplification driven by Arctic Ocean-mediated seasonal energy transfer. *Earth's Future*, 9(2), e2020EF001898.
- Chylek, P., Folland, C., Klett, J.D., Wang, M., Hengartner, N., Lesins, G. and Dubey, M.K. (2022) Annual mean Arctic amplification 1970–2020: observed and simulated by CMIP6 climate models. *Geophysical Research Letters*, 49(13), e2022GL099371.
- Dai, A., Luo, D., Song, M. and Liu, J. (2019) Arctic amplification is caused by sea-ice loss under increasing CO₂. *Nature Communications*, 10(1), 121. <https://doi.org/10.1038/s41467-018-07954-9>
- Dai, H. (2021) Roles of surface albedo, surface temperature and carbon dioxide in the seasonal variation of Arctic amplification. *Geophysical Research Letters*, 48(4). <https://doi.org/10.1029/2020GL090301>
- Danabasoglu, G. (2019a) NCAR CESM2 model output prepared for CMIP6 CMIP historical. Versions 20190308, 20190311, 20190514.
- Danabasoglu, G. (2019b) NCAR CESM2-WACCM model output prepared for CMIP6 ScenarioMIP ssp245. Version 20200528.
- Danabasoglu, G. (2019c) NCAR CESM2-WACCM Model Output Prepared for CMIP6 CMIP Historical.
- Danabasoglu, G. (2019d) NCAR CESM2-WACCM Model Output Prepared for CMIP6 ScenarioMIP ssp245.
- Danabasoglu, G., Lamarque, J.-F., Bacmeister, J., Bailey, D.A., DuVivier, A.K., Edwards, J., Emmons, L.K., Fasullo, J., Garcia, R., Gettelman, A., Hannay, C., Holland, M.M., Large, W.G., Lauritzen, P.H., Lawrence, D.M., Lenaerts, J.T.M., Lindsay, K., Lipscomb, W.H., Mills, M.J., Neale, R., Oleson, K.W., Otto-Bliesner, B., Phillips, A.S., Sacks, W., Tilmes, S., Kampenhout, L., Vertenstein, M., Bertini, A., Dennis, J., Deser, C., Fischer, C., Fox-Kemper, B., Kay, J.E., Kinnison, D., Kushner, P.J., Larson, V.E., Long, M.C., Mickelson, S., Moore, J.K., Nienhouse, E., Polvani, L., Rasch, P.J. and Strand, W.G. (2020) The Community Earth System Model version 2 (CESM2). *Journal of Advances in Modeling Earth Systems*, 12(2). <https://doi.org/10.1029/2019MS001916>
- Davy, R., Chen, L. and Hanna, E. (2018) Arctic amplification metrics. *International Journal of Climatology*, 38(12), 4384–4394.
- Decuyper, M., Tremblay, L.B. and Dufour, C.O. (2022) Impact of ocean heat transport on Arctic sea ice variability in the GFDL CM2-O model suite. *Journal of Geophysical Research, Oceans*, 127(3). <https://doi.org/10.1029/2021JC017762>
- Dix, M., Bi, D., Dobrohotoff, P., Fiedler, R., Harman, I., Law, R., Mackallah, C., Marsland, S., O'Farrell, S., Rashid, H., Srbinovsky, J., Sullivan, A., Trenham, C., Vohralik, P., Watterson, I., Williams, G., Woodhouse, M., Bodman, R., Dias, F.B., Domingues, C., Hannah, N., Heerdegen, A., Savita, A., Wales, S., Allen, C., Druken, K., Evans, B., Richards, C., Ridzwan, S.M., Roberts, D., Smillie, J., Snow, K., Ward, M. and Yang, R. (2019a) CSIRO-ARCCSS ACCESS-CM2 model output prepared for CMIP6 CMIP historical. Versions 20191108, 20191125, 20200306, 20210607.
- Dix, M., Bi, D., Dobrohotoff, P., Fiedler, R., Harman, I., Law, R., Mackallah, C., Marsland, S., O'Farrell, S., Rashid, H., Srbinovsky, J., Sullivan, A., Trenham, C., Vohralik, P., Watterson, I., Williams, G., Woodhouse, M., Bodman, R., Dias, F.B., Domingues, C.M., Hannah, N., Heerdegen, A., Savita, A., Wales, S., Allen, C., Druken, S.M., Roberts, D., Smillie, J., Snow, K., Ward, M. and Yang, R. (2019b) CSIRO-ARCCSS ACCESS-CM2 model output prepared for CMIP6 ScenarioMIP ssp245. Versions 20191108, 20200303, 20200428, 20210712, 20210802.
- Docquier, D. and Koenigk, T. (2021) A review of interactions between ocean heat transport and Arctic sea ice. *Environmental Research Letters*, 16(12), 123002.
- Docquier, D., Koenigk, T., Fuentes-Franco, R., Karami, M.P. and Ruprich-Robert, Y. (2021) Impact of ocean heat transport on the Arctic sea-ice decline: a model study with EC-Earth3. *Climate Dynamics*, 56(5-6), 1407–1432.
- Döscher, R., Acosta, M., Alessandri, A., Anthoni, P., Arsouze, T., Bergman, T., Bernardello, R., Boussetta, S., Caron, L.-P., Carver, G., Castrillo, M., Catalano, F., Cvijanovic, I., Davini, P., Dekker, E., Doblas-Reyes, F.J., Docquier, D., Echevarria, P., Fladrich, U., Fuentes-Franco, R., Gröger, M., Hardenberg, J.v., Hieronymus, J., Karami, M.P., Keskinen, J.-P., Koenigk, T., Makkonen, R., Massonnet, F., Ménégos, M., Miller, P.A., Moreno-Chamarro, E., Nieradzik, L., van Noije, T., Nolan, P., O'Donnell, D., Ollinaho, P., van den Oord, G., Ortega, P., Prims, O.T., Ramos, A., Reerink, T., Rousset, C., Ruprich-Robert, Y., Sager, P.L., Schmith, T., Schrödner, R., Serva, F., Sicardi, V., Madsen, M.S., Smith, B., Tian, T., Tourigny, E., Uotila, P., Vancoppenolle, M., Wang, S., Wärlind, D., Willén, U., Wyser, K., Yang, S., Yepes-Arbós, X. and Zhang, Q. (2022) The EC-Earth3 earth system model for the Coupled Model Intercomparison Project 6. *Geoscientific Model Development*, 15(7), 2973–3020.
- EC-Earth Consortium. (2019a) EC-Earth-Consortium EC-Earth3 model output prepared for CMIP6 CMIP historical.
- EC-Earth Consortium. (2019b) EC-Earth-Consortium EC-Earth3 model output prepared for CMIP6 ScenarioMIP ssp245.
- EC-Earth Consortium. (2019c) EC-Earth-Consortium EC-Earth3 model output prepared for CMIP6 ScenarioMIP ssp245.
- EC-Earth Consortium. (2021) EC-Earth-Consortium EC-Earth-3-CC model output prepared for CMIP6 CMIP historical.
- England, M.R., Eisenman, I., Lutsko, N.J. and Wagner, T.J.W. (2021) The recent emergence of Arctic amplification. *Geophysical Research Letters*, 48(15). <https://doi.org/10.1029/2021GL094086>
- Eyring, V., Bony, S., Meehl, G.A., Senior, C.A., Stevens, B., Stouffer, R.J. and Taylor, K.E. (2016) Overview of the Coupled Model Intercomparison Project phase 6 (CMIP6) experimental design and organization. *Geoscientific Model Development*, 9, 1937–1958.
- Good, P., Sellar, A., Tang, Y., Rumbold, S., Ellis, R., Kelley, D. and Kuhlbrodt, T. (2019) MOHC UKESM1.0-LL model output prepared for CMIP6 ScenarioMIP ssp245. Version 20210507, 20190715, 20190718, 20190801, 20190815, 20190510.
- Goosse, H., Kay, J.E., Armour, K.C., Bodas-Salcedo, A., Chepfer, H., Docquier, D., Jonko, A., Kushner, P.J., Lecomte, O., Massonnet, F., Park, H.-S., Pithan, F., Svensson, G. and Vancoppenolle, M. (2018) Quantifying climate feedbacks in polar regions. *Nature Communications*, 9(1). <https://doi.org/10.1038/s41467-018-04173-0>
- Hahn, L.C., Armour, K.C., Battisti, D.S., Donohoe, A., Pauling, A.G. and Bitz, C.M. (2020) Antarctic elevation drives hemispheric asymmetry in polar lapse rate climatology and feedback. *Geophysical Research Letters*, 47(16). <https://doi.org/10.1029/2020GL088965>

- Hajima, T., Abe, M., Arakawa, O., Suzuki, T., Komuro, Y., Ogura, T., Ogochi, K., Watanabe, M., Yamamoto, A., Tatebe, H., Noguchi, M.A., Ohgaito, R., Ito, A., Yamazaki, D., Ito, A., Takata, K., Watanabe, S., Kawamiya, M. and Tachiiri, K. (2019) MIROC MIROC-ES2L model output prepared for CMIP6 CMIP historical.
- Hajima, T., Watanabe, M., Yamamoto, A., Tatebe, H., Noguchi, M.A., Abe, M., Ohgaito, R., Ito, A., Yamazaki, D., Okajima, H., Ito, A., Takata, K., Ogochi, K., Watanabe, S. and Kawamiya, M. (2020) Development of the MIROC-ES2L earth system model and the evaluation of biogeochemical processes and feedbacks. *Geoscientific Model Development*, 13(5), 2197–2244.
- Holland, M.M. and Bitz, C.M. (2003) Polar amplification of climate change in coupled models. *Climate Dynamics*, 21(3–4), 221–232.
- Jenkins, M. and Dai, A. (2021) The impact of sea-ice loss on Arctic climate feedbacks and their role for Arctic amplification. *Geophysical Research Letters*, 48(15), e2021GL094599.
- Kelley, M., Schmidt, G.A., Nazarenko, L.S., Bauer, S.E., Ruedy, R., Russell, G.L., Ackerman, A.S., Aleinov, I., Bauer, M., Bleck, R., Canuto, V., Cesana, G., Cheng, Y., Clune, T.L., Cook, B.I., Cruz, C.A., Genio, A.D.D., Elsaesser, G.S., Faluvegi, G., Kiang, N.Y., Kim, D., Lacis, A.A., Leboissetier, A., LeGrande, A.N., Lo, K.K., Marshall, J., Matthews, E.E., McDermid, S., Mezuman, K., Miller, R.L., Murray, L.T., Oinas, V., Orbe, C., García-Pando, C.P., Perlwitz, J.P., Puma, M.J., Rind, D., Romanou, A., Shindell, D.T., Sun, S., Tausnev, N., Tsigaridis, K., Tselioudis, G., Weng, E., Wu, J. and Yao, M.-S. (2020) GISS-E2.1: configurations and climatology. *Journal of Advances in Modeling Earth Systems*, 12(8). <https://doi.org/10.1029/2019MS002025>
- Koenigk, T. and Brodeau, L. (2013) Ocean heat transport into the arctic in the twentieth and twenty-first century in EC-earth. *Climate Dynamics*, 42(11–12), 3101–3120.
- Lee, J., Kim, J., Sun, M.-A., Kim, B.-H., Moon, H., Sung, H.M., Kim, J. and Byun, Y.-H. (2019) Evaluation of the Korea Meteorological Administration Advanced Community Earth-system model (K-ACE). *Asia-Pacific Journal of Atmospheric Sciences*, 56(3), 381–395.
- Li, L. (2019a) CAS FGOALS-g3 model output prepared for CMIP6 CMIP historical.
- Li, L. (2019b) CAS FGOALS-g3 model output prepared for CMIP6 ScenarioMIP ssp245.
- Li, L., Yu, Y., Tang, Y., Lin, P., Xie, J., Song, M., Dong, L., Zhou, T., Liu, L., Wang, L., Pu, Y., Chen, X., Chen, L., Xie, Z., Liu, H., Zhang, L., Huang, X., Feng, T., Zheng, W., Xia, K., Liu, H., Liu, J., Wang, Y., Wang, L., Jia, B., Xie, F., Wang, B., Zhao, S., Yu, Z., Zhao, B. and Wei, J. (2020) The flexible Global Ocean-Atmosphere-Land System model grid-point version 3 (FGOALS-g3): description and evaluation. *Journal of Advances in Modeling Earth Systems*, 12(9). <https://doi.org/10.1029/2019MS002012>
- Liang, Y.-C., Polvani, L.M. and Mitevski, I. (2022) Arctic amplification, and its seasonal migration, over a wide range of abrupt CO₂ forcing. *NPJ Climate and Atmospheric Science*, 5(1). <https://doi.org/10.1038/s41612-022-00228-8>
- Madonna, E. and Sandø, A.B. (2021) Understanding differences in North Atlantic poleward ocean heat transport and its variability in global climate models. *Geophysical Research Letters*, 49(1). <https://doi.org/10.1029/2021GL096683>
- Manabe, S. and Wetherald, R.T. (1975) The effects of doubling the CO₂ concentration on climate of a general circulation model. *Journal of the Atmospheric Sciences*, 32, 3–15.
- Mauritsen, T., Bader, J., Becker, T., Behrens, J., Bittner, M., Brokopf, R., Brovkin, V., Claussen, M., Crueger, T., Esch, M., Fast, I., Fiedler, S., Fläschner, D., Gayler, V., Giorgetta, M., Goll, D.S., Haak, H., Hagemann, S., Hedemann, C., Hohenegger, C., Ilyina, T., Jahns, T., Cuesta, D.J.d.-l., Jungclaus, J., Kleinen, T., Kloster, S., Kracher, D., Kinne, S., Kleberg, D., Lasslop, G., Kornblueh, L., Marotzke, J., Matei, D., Meraner, K., Mikolajewicz, U., Modali, K., Möbis, B., Müller, W.A., Nabel, J.E.M.S., Nam, C.C.W., Notz, D., Nyawira, S.-S., Paulsen, H., Peters, K., Pincus, R., Pohlmann, H., Pongratz, J., Popp, M., Raddatz, T.J., Rast, S., Redler, R., Reick, C.H., Rohrschneider, T., Schemann, V., Schmidt, H., Schnur, R., Schulzweida, U., Six, K.D., Stein, L., Stemmler, I., Stevens, B., Storch, J.-S., Tian, F., Voigt, A., Vrese, P., Wieners, K.-H., Wilken-skjeld, S., Winkler, A. and Roeckner, E. (2019) Developments in the MPI-M earth system model version 1.2 (MPI-ESM1.2) and its response to increasing CO₂. *Journal of Advances in Modeling Earth Systems*, 11(4), 998–1038.
- Metzner, E.P., Salzmann, M. and Gerdes, R. (2020) Arctic Ocean surface energy flux and the cold halocline in future climate projections. *Journal of Geophysical Research, Oceans*, 125(2), e2019JC015554. <https://doi.org/10.1029/2019JC015554>.
- Miller, G.H., Alley, R.B., Brigham-Grette, J., Fitzpatrick, J.J., Polyak, L., Serreze, M.C. and White, J.W.C. (2010) Arctic amplification: can the past constrain the future? *Quaternary Science Reviews*, 29(15–16), 1779–1790.
- NASA/GISS. (2018a) NASA-GISS GISS-E2.1G model output prepared for CMIP6 CMIP historical.
- NASA/GISS. (2018b) NASA-GISS GISS-E2.1H model output prepared for CMIP6 CMIP.
- NASA/GISS. (2019a) NASA-GISS GISS-E2. 1H model output prepared for CMIP6 CMIP historical.
- NASA/GISS. (2019b) NASA-GISS GISS-E2-2-G model output prepared for CMIP6 CMIP historical.
- NASA/GISS. (2019c) NASA-GISS GISS-E2-2-G model output prepared for CMIP6 CMIP.
- NASA/GISS. (2020) NASA-GISS GISS-E2. 1G model output prepared for CMIP6 ScenarioMIP ssp245.
- Park, H.-S., Kim, S.-J., Stewart, A.L., Son, S.-W. and Seo, K.-H. (2019) Mid-holocene northern hemisphere warming driven by Arctic amplification. *Science Advances*, 5(12), eaax8203.
- Pithan, F. and Mauritsen, T. (2014) Arctic amplification dominated by temperature feedbacks in contemporary climate models. *Nature Geoscience*, 7(3), 181–184.
- Previdi, M., Smith, K.L. and Polvani, L.M. (2021) Arctic amplification of climate change: A review of underlying mechanisms. *Environmental Research Letters*, 16(9), 093003.
- Rind, D., Orbe, C., Jonas, J., Nazarenko, L., Zhou, T., Kelley, M., Lacis, A., Shindell, D., Faluvegi, G., Romanou, A., Russell, G., Tausnev, N., Bauer, M. and Schmidt, G. (2020) GISS model E2.2: a climate model optimized for the middle atmosphere—model structure, climatology, variability, and climate sensitivity. *Journal of Geophysical Research – Atmospheres*, 125(10). <https://doi.org/10.1029/2019JD032204>
- Salzmann, M. (2017) The polar amplification asymmetry: role of antarctic surface height. *Earth System Dynamics*, 8(2), 323–336.
- Seferian, R. (2018) CNRM-CERFACS CNRM-ESM2-1 model output prepared for CMIP6 CMIP historical. Versions 20181206, 20190125, 20200117, 20200408.
- Séférian, R., Nabat, P., Michou, M., Saint-Martin, D., Voldoire, A., Colin, J., Decharme, B., Delire, C., Berthet, S., Chevallier, M.,

- Sénési, S., Franchisteguy, L., Vial, J., Mallet, M., Joetzier, E., Geofroy, O., Guérémy, J.-F., Moine, M.-P., Msadek, R., Ribes, A., Rocher, M., Roehrig, R., Méliá, D.S.Y., Sanchez, E., Terray, L., Valcke, S., Waldman, R., Aumont, O., Bopp, L., Deshayes, J., Éthé, C. and Madec, G. (2019) Evaluation of CNRM earth system model, CNRM-ESM2-1: role of earth system processes in present-day and future climate. *Journal of Advances in Modeling Earth Systems*, 11(12), 4182–4227.
- Seland, Ø., Bentsen, M., Olivie, D., Toniazzo, T., Gjermundsen, A., Graff, L.S., Debernard, J.B., Gupta, A.K., He, Y.-C., Kirkevåg, A., Schwinger, J., Tjiputra, J., Aas, K.S., Bethke, I., Fan, Y., Griesfeller, J., Grini, A., Guo, C., Ilicak, M., Karset, I.H.H., Landgren, O., Liakka, J., Moseid, K.O., Nummelin, A., Spensberger, C., Tang, H., Zhang, Z., Heinze, C., Iversen, T. and Schulz, M. (2020) Overview of the Norwegian Earth System Model (NorESM2) and key climate response of CMIP6 DECK, historical, and scenario simulations. *Geoscientific Model Development*, 13(12), 6165–6200.
- Seland, Ø., Bentsen, M., Olivie, D.J.L., Toniazzo, T., Gjermundsen, A., Graff, L.S., Debernard, J.B., Gupta, A.K., He, Y., Kirkevåg, A., Schwinger, J., Tjiputra, J., Aas, K.S., Bethke, I., Fan, Y., Griesfeller, J., Grini, A., Guo, C., Ilicak, M., Karset, I.H.H., Landgren, O.A., Liakka, J., Moseid, K.O., Nummelin, A., Spensberger, C., Tang, H., Zhang, Z., Heinze, C., Iversen, T. and Schulz, M. (2019a) NCC NorESM2-LM model output prepared for CMIP6 ScenarioMIP ssp245. Version 20191108.
- Seland, Ø., Bentsen, M., Olivie, D.J.L., Toniazzo, T., Gjermundsen, A., Graff, L.S., Debernard, J.B., Gupta, A.K., He, Y., Kirkevåg, A., Schwinger, J., Tjiputra, J., Aas, K.S., Bethke, I., Fan, Y., Griesfeller, J., Grini, A., Guo, C., Ilicak, M., Karset, I.H.H., Landgren, O.A., Liakka, J., Moseid, K.O., Nummelin, A., Spensberger, C., Tang, H., Zhang, Z., Heinze, C., Iversen, T. and Schulz, M. (2019b) NCC NorESM2-LM model output prepared for CMIP6 CMIP historical. Versions 20190815, 20190920.
- Sellar, A.A., Jones, C.G., Mulcahy, J.P., Tang, Y., Yool, A., Wiltshire, A., O'Connor, F.M., Stringer, M., Hill, R., Palmieri, J., Woodward, S., Mora, L., Kuhlbrodt, T., Rumbold, S.T., Kelley, D.I., Ellis, R., Johnson, C.E., Walton, J., Abraham, N.L., Andrews, M.B., Andrews, T., Archibald, A.T., Berthou, S., Burke, E., Blockley, E., Carslaw, K., Dalvi, M., Edwards, J., Folberth, G.A., Gedney, N., Griffiths, P.T., Harper, A.B., Hendry, M.A., Hewitt, A.J., Johnson, B., Jones, A., Jones, C.D., Keeble, J., Liddicoat, S., Morgenstern, O., Parker, R.J., Predoi, V., Robertson, E., Siahann, A., Smith, R.S., Swaminathan, R., Woodhouse, M.T., Zeng, G. and Zerroukat, M. (2019) UKESM1: description and evaluation of the UK Earth System Model. *Journal of Advances in Modeling Earth Systems*, 11(12), 4513–4558.
- Serreze, M.C. and Francis, J.A. (2006) The arctic amplification debate. *Climatic Change*, 76(3–4), 241–264.
- Shim, S., Lim, Y.-J., Byun, Y.-H., Seo, J., Kwon, S. and Kim, B.-H. (2020) NIMS-KMA UKESM1.0-LL model output prepared for CMIP6 ScenarioMIP ssp245. Version, 20200818.
- Shiogama, H., Abe, M. and Tatebe, H. (2019) MIROC MIROC6 model output prepared for CMIP6 ScenarioMIP ssp245.
- Singh, H. A., & Polvani, L. M. (2020). Low Antarctic continental climate sensitivity due to high ice sheet orography. *Npj Climate and Atmospheric Science*, 3(1). <https://doi.org/10.1038/s41612-020-00143-w>
- Song, Z., Qiao, F., Bao, Y., Shu, Q., Song, Y. and Yang, X. (2019a) FIO-QLNM FIO-ESM2.0 model output prepared for CMIP6 CMIP historical.
- Song, Z., Qiao, F., Bao, Y., Shu, Q., Song, Y. and Yang, X. (2019b) FIO-QLNM FIO-ESM2.0 model output prepared for CMIP6 ScenarioMIP.
- Swart, N.C., Cole, J.N., Kharin, V.V., Lazare, M., Scinocca, J.F., Gillett, N.P., Anstey, J., Arora, V., Christian, J.R., Jiao, Y., Lee, W.G., Majaess, F., Saenko, O.A., Seiler, C., Seinen, C., Shao, A., Solheim, L., von Salzen, K., Yang, D., Winter, B. and Sigmund, M. (2019a) CCCma CanESM5 model output prepared for CMIP6 ScenarioMIP ssp245. Version 20190429.
- Swart, N.C., Cole, J.N., Kharin, V.V., Lazare, M., Scinocca, J.F., Gillett, N.P., Anstey, J., Arora, V., Christian, J.R., Jiao, Y., Lee, W.G., Majaess, F., Saenko, O.A., Seiler, C., Seinen, C., Shao, A., Solheim, L., von Salzen, K., Yang, D., Winter, B. and Sigmund, M. (2019b) CCCma CanESM5-CanOE model output prepared for CMIP6 CMIP historical.
- Swart, N.C., Cole, J.N., Kharin, V.V., Lazare, M., Scinocca, J.F., Gillett, N.P., Anstey, J., Arora, V., Christian, J.R., Jiao, Y., Lee, W.G., Majaess, F., Saenko, O.A., Seiler, C., Seinen, C., Shao, A., Solheim, L., von Salzen, K., Yang, D., Winter, B. and Sigmund, M. (2019c) CCCma CanESM5-CanOE model output prepared for CMIP6 ScenarioMIP.
- Swart, N.C., Cole, J.N., Kharin, V.V., Lazare, M., Scinocca, J.F., Gillett, N.P., Anstey, J., Arora, V., Christian, J.R., Jiao, Y., Lee, W.G., Majaess, F., Saenko, O.A., Seiler, C., Seinen, C., Shao, A., Solheim, L., von Salzen, K., Yang, D., Winter, B. and Sigmund, M. (2019d) CCCma CanESM5 model output prepared for CMIP6 CMIP historical. Version 20190429.
- Swart, N.C., Cole, J.N.S., Kharin, V.V., Lazare, M., Scinocca, J.F., Gillett, N.P., Anstey, J., Arora, V., Christian, J.R., Hanna, S., Jiao, Y., Lee, W.G., Majaess, F., Saenko, O.A., Seiler, C., Seinen, C., Shao, A., Sigmund, M., Solheim, L., von Salzen, K., Yang, D. and Winter, B. (2019e) The Canadian Earth System Model version 5 (CanESM5.0.3). *Geoscientific Model Development*, 12(11), 4823–4873.
- Tachiiri, K., Abe, M., Hajima, T., Arakawa, O., Suzuki, T., Komuro, Y., Ogochi, K., Watanabe, M., Yamamoto, A., Tatebe, H., Noguchi, M.A., Ohgaito, R., Ito, A., Yamazaki, D., Ito, A., Takata, K., Watanabe, S. and Kawamiya, M. (2019) MIROC MIROC-ES2L model output prepared for CMIP6 ScenarioMIP ssp245.
- Tang, Y., Rumbold, S., Ellis, R., Kelley, D., Mulcahy, J., Sellar, A., Walton, J. and Jones, C. (2019) MOHC UKESM1.0-LL model output prepared for CMIP6 CMIP historical. Versions 20190406, 20190627, 20190502, 20190708, 20190510, 20191115, 20190604, 20191113, 20190603, 20191011, 20191015, 20191213, 20191209, 20191210, 20191119.
- Tatebe, H., Ogura, T., Nitta, T., Komuro, Y., Ogochi, K., Takemura, T., Sudo, K., Sekiguchi, M., Abe, M., Saito, F., Chikira, M., Watanabe, S., Mori, M., Hirota, N., Kawatani, Y., Mochizuki, T., Yoshimura, K., Takata, K., O'ishi, R., Yamazaki, D., Suzuki, T., Kurogi, M., Kataoka, T., Watanabe, M. and Kimoto, M. (2019) Description and basic evaluation of simulated mean state, internal variability, and climate sensitivity in MIROC6. *Geoscientific Model Development*, 12(7), 2727–2765.
- Tatebe, H. and Watanabe, M. (2018) MIROC MIROC6 model output prepared for CMIP6 CMIP historical. Versions 20181212, 20190311, 20200519.
- Tsubouchi, T., Våge, K., Hansen, B., Larsen, K.M.H., Østerhus, K., Johnson, C., Jónsson, S. and Valdimarsson, H. (2020) Increased ocean heat transport into the Nordic Seas and Arctic Ocean over the period 1993–2016. *Nature Climate Change*, 11(1), 21–26.

- van der Linden, E.C., Bars, D.L., Bintanja, R. and Hazeleger, W. (2019) Oceanic heat transport into the Arctic under high and low CO₂ forcing. *Climate Dynamics*, 53(7-8), 4763–4780.
- Voltaire, A. (2018) CMIP6 simulations of the CNRM-CERFACS based on CNRM-CM6-1 model for CMIP experiment historical. Versions 20180917, 20181126, 20190125, 20191004, 20200529.
- Voltaire, A. (2019a) CNRM-CERFACS CNRM-CM6-1 model output prepared for CMIP6 scenario MIP ssp245. Versions 20190219, 20190410, 20200212.
- Voltaire, A. (2019b) CNRM-CERFACS CNRM-ESM2-1 model output prepared for CMIP6 ScenarioMIP ssp245. Versions 20190328, 20190410, 20201028.
- Voltaire, A., Saint-Martin, D., S n si, S., Decharme, B., Alias, A., Chevallier, M., Colin, J., Gu r my, J.-F., Michou, M., Moine, M.-P., Nabat, P., Roehrig, R., M lia, D.S.y., S f rian, R., Valcke, S., Beau, I., Belamari, S., Berthet, S., Cassou, C., Cattiaux, J., Deshayes, J., Douville, H., Eth , C., Franchist guy, L., Geoffroy, O., L vy, C., Madec, G., Meurdesoif, Y., Msadek, R., Ribes, A., Sanchez-Gomez, E., Terray, L. and Waldman, R. (2019) Evaluation of CMIP6 DECK experiments with CNRM-CM6-1. *Journal of Advances in Modeling Earth Systems*, 11(7), 2177–2213.
- Walsh, J.E., Fetterer, F., Stewart, J.S., and Chapman, W.L. (2017) A database for depicting Arctic sea ice variations back to 1850. *Geographical Review*, 107(1), 89–107.
- Wieners, K.-H., Giorgetta, M., Jungclaus, J., Reick, C., Esch, M., Bittner, M., Gayler, V., Haak, H., de Vrese, P., Raddatz, T., Mauritsen, T., von Storch, J.-S., Behrens, J., Brovkin, V., Claussen, M., Crueger, T., Fast, I., Fiedler, S., Hagemann, S., Hohenegger, C., Jahns, T., Kloster, S., Kinne, S., Lasslop, G., Kornbl uh, L., Marotzke, J., Matei, D., Meraner, K., Mikolajewicz, U., Modali, K., M ller, W., Nabel, J., Notz, D., Peters-von Gehlen, K., Pincus, R., Pohlmann, H., Pongratz, J., Rast, S., Schmidt, H., Schnur, R., Schulzweida, U., Six, K., Stevens, B., Voigt, A. and Roeckner, E. (2019a) MPI-M MPI-ESM1.2-LR model output prepared for CMIP6 ScenarioMIP ssp245. Versions 20190710, 20210901.
- Wieners, K.-H., Giorgetta, M., Jungclaus, J., Reick, C., Esch, M., Bittner, M., Legutke, S., Schupfner, M., Wachsmann, F., Gayler, V., Haak, H., de Vrese, P., Raddatz, T., Mauritsen, T., von Storch, J.-S., Behrens, J., Brovkin, V., Claussen, M., Crueger, T., Fast, I., Fiedler, S., Hagemann, S., Hohenegger, C., Jahns, T., Kloster, S., Kinne, S., Lasslop, G., Kornbl uh, L., Marotzke, J., Matei, D., Meraner, K., Mikolajewicz, U., Modali, K., M ller, W., Nabel, J., Notz, D., Peters-von Gehlen, K., Pincus, R., Pohlmann, H., Pongratz, J., Rast, S., Schmidt, H., Schnur, R., Schulzweida, U., Six, K., Stevens, B., Voigt, A. and Roeckner, E. (2019b) MPI-M MPI-ESM1.2-LR model output prepared for CMIP6 CMIP historical. Versions 20190710, 20210901.
- Ye, K. and Messori, G. (2021) Inter-model spread in the wintertime Arctic amplification in the CMIP6 models and the important role of internal climate variability. *Global and Planetary Change*, 204, 103543.
- Ziehn, T., Chamberlain, M., Lenton, A., Law, R., Bodman, R., Dix, M., Wang, Y., Dobrohotoff, P., Srbinovsky, J., Stevens, L., Vohralik, P., Mackallah, C., Sullivan, A., O'Farrell, S. and Druken, K. (2019a) CSIRO ACCESS-ESM1.5 model output prepared for CMIP6 CMIP historical.
- Ziehn, T., Chamberlain, M., Lenton, A., Law, R., Bodman, R., Dix, M., Wang, Y., Dobrohotoff, P., Srbinovsky, J., Stevens, L., Vohralik, P., Mackallah, C., Sullivan, A., O'Farrell, S. and Druken, K. (2019b) CSIRO ACCESS-ESM1.5 model output prepared for CMIP6 ScenarioMIP ssp245.
- Ziehn, T., Chamberlain, M.A., Law, R.M., Lenton, A., Bodman, R.W., Dix, M., Stevens, L., Wang, Y.-P. and Srbinovsky, J. (2020) The Australian Earth System Model: ACCESS-ESM1.5. *Journal of Southern Hemisphere Earth Systems Science*, 70(1), 193.

SUPPORTING INFORMATION

Additional supporting information can be found online in the Supporting Information section at the end of this article.

How to cite this article: Hajjar, K. & Salzmann, M. (2023) Relative contributions of local heat storage and ocean heat transport to cold-season Arctic Ocean surface energy fluxes in CMIP6 models. *Quarterly Journal of the Royal Meteorological Society*, 149(755), 2091–2106. Available from: <https://doi.org/10.1002/qj.4496>